Supporting Information

Hagmann et al. 10.1073/pnas.1009073107

SI Materials and Methods

Structural Connectivity Mapping. The path from q-ball imaging to structural connection matrix is made of several processing steps that are described in detail elsewhere (1) and include gray and white matter segmentation, partition of the gray matter in multiple regions of interest (ROI) and tractography between each pairs of ROIs. We summarize the key steps and the specific aspects related to the present study.

(*i*) After the registration of the subject's T1-weighted image onto its b0 image, the former is processed with a freely available software called Freesurfer (surfer.nmr.mgh.harvard.edu). It produces outputs that correspond to segmentations of the white matter, the cortex, and the deep gray nuclei in the subject reference space (2).

(*ii*) The cortical mesh produced by the same software was used to produce two standardized partitions of the subject's cortex into (a) 66 anatomical regions and (b) 241 ROIs of approximately identical size (6 cm^2). These regions and ROIs are in anatomical correspondence between subjects thanks to a surface-based gyral pattern recognition algorithm (3).

(*iii*) In a third step in-house software was used to perform whole-brain streamline tractography inside the white matter mask obtained from the T1 segmentation using the ODF maps produced by the q-ball data. Q-ball data enable the mapping of fiber crossing, and fibers are initiated uniformly over the entire white matter mask (30 per mm^3). For every fiber the mean ADC, FA at b-value 1,000 and 3,000 s/mm^2, as well as its length, were computed.

(*iv*) Finally, we combined the results of steps (*ii*) and (*iii*) to create connection matrices of various kinds. Two ROIs are connected if at least one fiber connects them. The first connection matrix maps the connection density between ROIs and is calculated as a number of connections per unit surface $C = S^{-1} \Sigma_i 1/l(i)$, where S is the total surface of the two ROIs in question, Σ_i is the sum over all fibers connecting the two ROIs, and the correction term l(i) in the denominator is the length of a specific fiber and was introduced to remove the linear bias toward longer fibers. The second matrix maps the average b = 3,000 ADC along a connection linking two ROIs.

(*v*) We also obtained low-resolution matrices with respect to the 66 cortical regions by averaging the values of the connections obtained at high resolution.

Network Metrics. All graph theoretical analyses were carried out on weighted SC using the Brain Connectivity Toolbox, as described in ref. 4. Node strength was computed as the sum of all of the edge weights attached to each node. The clustering coefficient was computed according to ref. 5, and the path length was computed from the weighted distance matrix. Both clustering and path length were scaled against values obtained from populations of 100 randomly rewired graphs that preserved node degrees and approximated node strength. This comparison yields a coefficient that expresses the level of clustering or path length in the empirical network relative to a null population with preserved node statistics but scrambled global topology. The ratio of scaled clustering to scaled path length provided the small-world index (6), with a value >>1 indicative of the presence of small-world attributes. Global efficiency was computed according to ref. 7, and node betweenness centrality was derived from the set of shortest path spanning the network (8). An optimization algorithm was applied to identify an optimal partitioning of the network into modules such that the modularity score (9) was maximized. Different module partitions across subjects were compared by computing their normalized mutual information (10), which ranges between 0 (independence) and 1 (identical partitions).

1. Hagmann P, et al. (2008) Mapping the structural core of human cerebral cortex. *PLoS Biol* 6:e159.
2. Fischl B, et al. (2002) Whole brain segmentation: Automated labeling of neuroanatomical structures in the human brain. *Neuron* 33:341–355.
3. Fischl B, et al. (2004) Automatically parcellating the human cerebral cortex. *Cereb Cortex* 14:11–22.
4. Rubinov M, Sporns O (2010) Complex network measures of brain connectivity: uses and interpretations. *Neuroimage* 52:1059–1069.
5. Onnela JP, Saramäki J, Kertész J, Kaski K (2005) Intensity and coherence of motifs in weighted complex networks. *Phys Rev E Stat Nonlin Soft Matter Phys* 71:065103.
6. Humphries MD, Gurney K (2008) Network 'small-world-ness': A quantitative method for determining canonical network equivalence. *PLoS ONE* 3:e0002051.
7. Latora V, Marchiori M (2001) Efficient behavior of small-world networks. *Phys Rev Lett* 87:198701.
8. Freeman LC (1978) Centrality in social networks: Conceptual clarification. *Soc Networks* 1:215–239.
9. Newman ME (2004) Fast algorithm for detecting community structure in networks. *Phys Rev E Stat Nonlin Soft Matter Phys* 69:066133.
10. Kuncheva L, Hadjotodorov S (2004) Using diversity in cluster ensembles. *IEEE Int Conf Syst Man Cybern* 1214–1219.

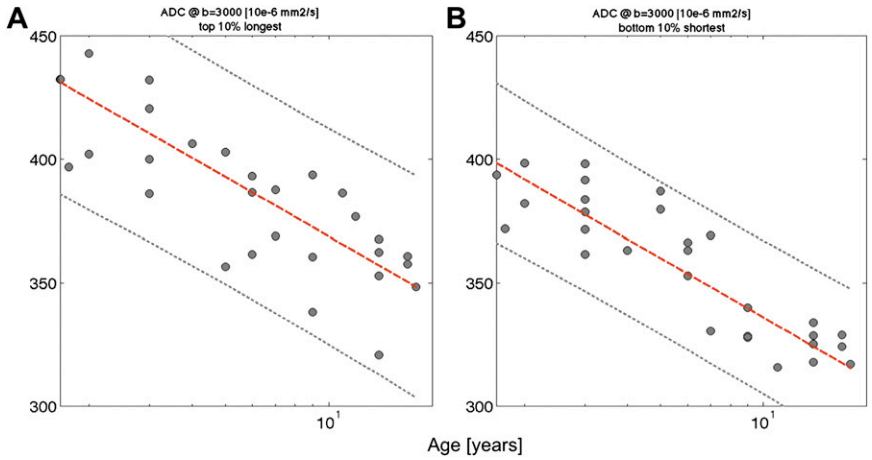

Fig. S1. Change of average connection apparent diffusion coefficient (ADC) measured at b = 3,000 s/mm^2 with respect to developmental age (*A*) for the top 10% longest fibers (linear regression provides an offset of 448 mm^2/s and a slope of −34.6); and (*B*) for the bottom 10% shortest fibers (linear regression provides an offset of 415 mm^2/s and a slope of −34.7).

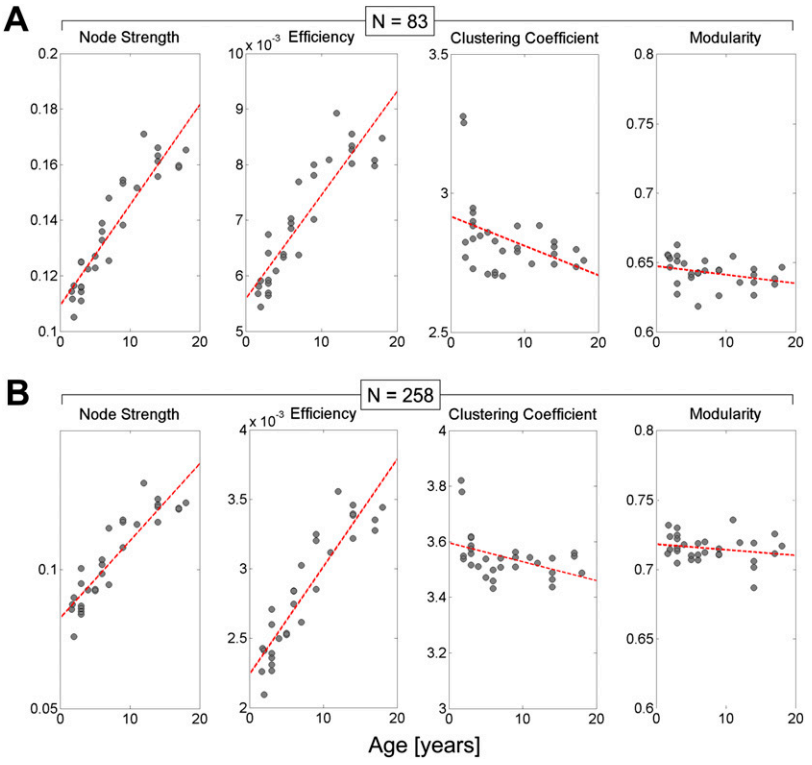

Fig. S2. Relationship of network metrics and developmental age. Results shown are for whole-brain networks at two spatial resolutions (n = 83 and n = 258 nodes). Scatter plots show node strength, global efficiency, clustering coefficient, and modularity (left to right). All measures are computed from the weighted structural connectivity matrices of individual subjects. Values for the clustering coefficient are scaled relative to populations of 100 random networks with preserved degree and weight distributions. For *R* and *P* values, see Table 1 in main text.

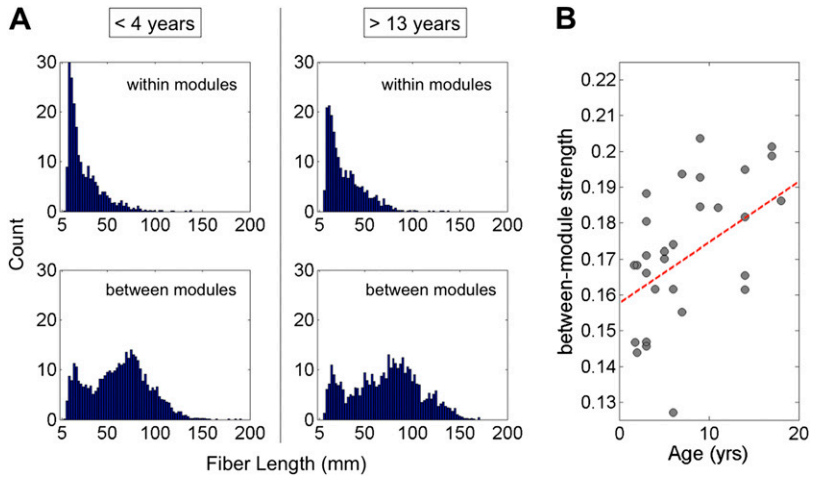

Fig. S3. Relation of connection length and efficacy to module boundaries. (*A*) Histograms of connection lengths of pathways linking pairs of nodes located within the same module ("within module") and in different modules ("between modules"), aggregated from participants <4 y of age (n = 10) and >13 y of age (n = 7). For both age groups, intramodular connections were found to be predominantly short, whereas intermodule connections extended over greater distances. Connection lengths were derived from the trajectories of tractography streamlines and were not corrected for differences in head/brain size. (*B*) When the total connection efficacy is divided into a within- and a between-module component, a significant developmental increase of efficacy for between-modules connections is revealed (R = 0.42, P < 0.05).

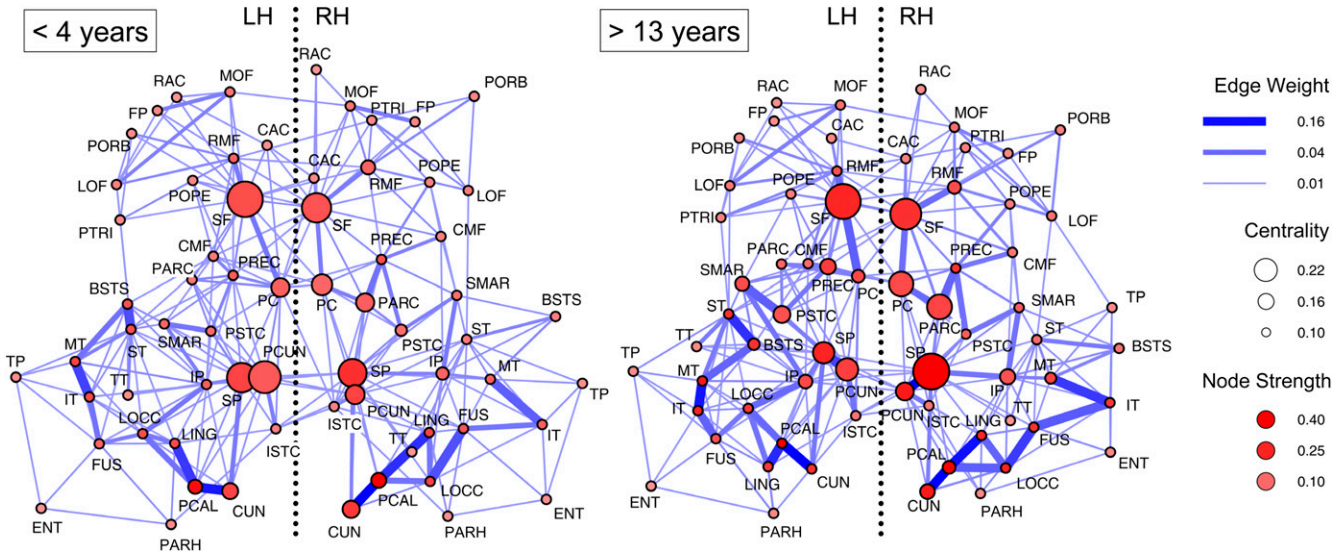

Fig. S4. Developmental changes in structural connectivity. The plots show a Kamada-Kawai force spring layout of the backbone of structural connectivity averaged over younger (<4 y) and older (>13 y) subjects. Plots show node strengths, edge weights, and betweenness centrality. Major hubs in superior frontal cortex, superior parietal cortex, and precuneus are evident in both younger and older brains. BSTS, bank of the superior temporal sulcus; CAC, caudal anterior cingulate cortex; CMF, caudal middle frontal cortex; CUN, cuneus; ENT, entorhinal cortex; FP, frontal pole; FUS, fusiform gyrus; IP, inferior parietal cortex; IT, inferior temporal cortex; ISTC, isthmus of the cingulate cortex; LOCC, lateral occipital cortex; LOF, lateral orbitofrontal cortex; LING, lingual gyrus; MOF, medial orbitofrontal cortex; MT, middle temporal cortex; PARC, paracentral lobule; PARH, parahippocampal cortex; POPE, pars opercularis; PORB, pars orbitalis; PTRI, pars triangularis; PCAL, pericalcarine cortex; PSTC, postcentral gyrus; PC, posterior cingulate cortex; PREC, precentral gyrus; PCUN, precuneus; RAC, rostral anterior cingulate cortex; RMF, rostral middle frontal cortex; SF, superior frontal cortex; SP, superior parietal cortex; ST, superior temporal cortex; SMAR, supramarginal gyrus; TP, temporal pole; TT, transverse temporal cortex.

Table S1. Subject status description

Patient no.	Sex	Age (y)	Diffusion MRI	MPRAGE	Resting-state fMRI	GA/NO	Reason for scanning	MRI structural findings
1	M	2	+	+	+	GA	Seizure	Small T2 hyperintense lesion found in splenium of corpus callosum, resolved on follow-up
2	F	3	+	+	+	GA	Fevers, recurrent otitis	Soft-tissue enhancement nasopharynx; normal brain
3	M	4	+	+	+	GA	Asymmetric skull, preferential right-sided vision	Normal
4	M	6	+	+	+	GA	Stiffness, R arm pronated, L arm flexed, eyes rolling back, EEG Shows R occipital spike at sleep	Normal
5	M	6	+	+	+	GA	Regression, ear infections, adenoids	Few nonspecific white matter foci of T2 hyperintensity
6	F	7	+	+	—	NO	Systemic lupus erythematosous, APLAB syndrome with headache, fatigue, new leg hyperreflexia	Normal
7	F	9	+	+	—	NO	Seizures	Normal
8	M	11	+	+	+	NO	X-linked hypophosphatemia, short stature, and right olivary lesion stable on multiple follow-ups	Stable exophytic lesion in right medullary olive, uncertain significance
9	M	12	+	+	—	NO	Cerebellar astrocytoma status post resection for follow-up	No tumor recurrence
10	F	14	+	+	+	NO	Episodic vomiting for 5 mo	Normal
11	F	14	+	+	+	NO	Headaches	Normal
12	M	14	+	+	+	GA	Seizures	Normal
13	F	18	+	+	+	NO	Headache, migratory sensory symptoms	Few nonspecific white matter foci of T2 hyperintensities
14	M	2	+	+	+	GA	Gait abnormalities	Normal
15	M	3	+	+	—	GA	Developmental delay	Normal
16	F	5	+	+	+	GA	Seizure status post right partial temporal pole resection	Stable postoperative changes
17	M	6	+	+	—	GA	Increased reflexes on the right	Normal
18	F	3	+	+	—	GA	Cough, shortness of breath, immobile vocal cords, tracheomalacia, reflux	Normal
19	F	2	+	+	—	GA	Seizures	Few focal T2 nonspecific hyperintensties
20	F	3	+	+	+	GA	Status post left-sided enucleation for resection of a retinoblastoma	Orbital postsurgical, no evidence of tumor recurrence
21	F	5	+	+	—	GA	Vomitting, unsteady gait	Normal
22	F	17	+	+	—		Post craniectomy follow-up	Postsurgical changes
23	F	9	+	+	—	NO	Headaches, psychiatric symptoms	Normal
24	M	1.65	+	+	—	GA	Developmental delay, motor difficulties	Normal
25	F	14	+	+	—	NO	Headache	Nonspecific focus of T2 hyperintensity in the left thalamus which resolved on follow-up
26	F	7	+	+	—	GA	Headaches	Normal
27	M	1.75	+	+	—	GA	No change in head circumference for 6 mo; difficulty swallowing; cognitive concerns	Normal
28	M	3	+	+	—	GA	Hypotonia, motor delays, wide-based gait	Normal
29	F	9	+	+	—	NO	Headaches; psychiatric symptoms	Normal
30	F	17	+	+	+	NO	Status post Chiari I decompression	Postsurg changes

Subjects not undergoing anesthesia could either cope with scanning on their own or where coached by a child life specialist before and during the scanning. Scan quality with respect to motion and artifacts was checked by two neuroradiolgists, and only good-quality scans were used for the study. MPRAGE, magnetization prepared rapid gradient echo; GA, general anesthesia; NO, no sedation/anesthesia; M, male; F, female; R, right; L, left; APLAB, antiphospholipid antibody.